Ab initio dynamical response of metal monolayers

A. Bergara
Materia Kondentsatuaren Fisika Saila, Zientzia Fakultatea, Euskal Herriko Unibertsitatea, 644 Posta Kutxatila, 48080 Bilbo, Basque Country, Spain

V. M. Silkin
Donostia International Physics Center (DIPC), Paseo de Manuel Lardizabal, 20018 San Sebastián/Donostia, Basque Country, Spain

E. V. Chulkov and P. M. Echenique
Dpto. de Física de Materiales and Centro Mixto CSIC-UPV/EHU, Facultad de Química, UPV/EHU, Apdo. 1072, 20080 San Sebastián/Donostia, Basque Country, Spain

(Received 24 January 2003; published 5 June 2003)

Ab initio calculation of the density response function within the random-phase approximation is presented for lithium, berillium, and boron freestanding metal monolayers (ML's). Although the monolayers manifest common features related to their reduced dimensionality, their different band structures lead to significant modifications in the density response function. Besides the common intraband and interband collective excitations, the beryllium ML also presents characteristic features of acoustic plasmons associated with the presence of two types of carriers at the Fermi level. Contrary to the bulk, long-wavelength intraband plasmons in lithium and beryllium ML's cannot decay via umklapp processes associated with the band structure. At the same time, these processes lead to a significant reduction of the momentum threshold for decay of these plasmons comparing with a free-electron two-dimensional gas model. It is also shown how a change of the symmetry of the boron ML modifies completely the character of the intraband plasmons.

DOI: 10.1103/PhysRevB.67.245402 PACS number(s): 68.35.−p, 73.20.−r, 73.21.−b

I. INTRODUCTION

Reduction of the dimensionality of an electron system leads to the appearance of properties that are different from those of bulk solids. Thus, dynamical screening of a two-dimensional (2D) electron gas is fundamentally different from that of a three-dimensional (3D) electron system. If in 3D the collective electron excitations have a nonzero minimum energy,[1] in 2D these modes have a well-known $\sqrt{q}$ dispersion for small momenta q.[2] Investigation of these low-energy collective excitations has been a subject of active experimental and theoretical research, especially for semiconductor heterostructures.[3] At the same time, investigations of collective excitations of 2D atomic structures are just at the beginning. Recent experiments performed for atomic coverages with $\theta \leqslant 1$ adlayers on semiconductors have revealed the two-dimensional collective excitations of the overlayers.[4,5] On the other hand, there are materials with a clear layered structure, i.e., graphite, high-temperature superconductors, and the recently discovered medium-temperature superconductor MgB_2,[6] which are characterized by a strong anisotropy. For example, in the latter compound boron monolayers (ML's) alternate with hexagonal layers of Mg atoms which donate their electrons to the boron planes and electron properties of MgB_2 are dominated by the electronic characteristics of boron ML's.

Contrary to situation in a strict 2D electon gas model well studied up to now, the ions confined in a ML interact via the full three-dimensional Coulomb potential: both the potential and electronic charge density are therefore allowed to extend out of the plane. An evident consequence of the planar confinement is the lower atomic coordination as compared to the bulk, and the expectation is that atoms in the ML should be less strongly bound. This change in the coordination number also has a profound effect on the electronic structure and, respectively, on the response function. Although some characteristics of the response function related to the dimensionality of the system are common for ML's, band structure features that depend on the valence of atoms and symmetry of ML's may lead to important distinctions.

In what follows, we present the evaluation of the *ab initio* dynamic response function within a random-phase approximation (RPA) for lithium, beryllium, and boron free ML's. In Sec. II we briefly describe the theoretical and computational methods that we have used. The calculation results and discussion are presented in Sec. III, and conclusions are given in Sec. IV. Unless otherwise stated, we use atomic units throughout, i.e., $e^2=\hbar=m_e=1$.

II. *Ab initio* DENSITY RESPONSE FUNCTION OF A MONOLAYER

In linear response theory the density response function, $\chi(\mathbf{r},\mathbf{r}';\omega)$, of an interacting electron system is defined by the equation

$$n^{\mathrm{ind}}(\mathbf{r},\omega)=\int d\mathbf{r}'\,\chi(\mathbf{r},\mathbf{r}';\omega)V^{\mathrm{ext}}(\mathbf{r}';\omega), \tag{1}$$

where $n^{\mathrm{ind}}(\mathbf{r},\omega)$ is the electron density induced by an external potential $V^{\mathrm{ext}}(\mathbf{r},\mathbf{r}';\omega)$. In the RPA,[1] the density response function satisfies the integral equation

$$\chi(\mathbf{r},\mathbf{r}';\omega)=\chi^0(\mathbf{r},\mathbf{r}';\omega) + \int d^3\mathbf{r}_1 \int d^3\mathbf{r}_2 \chi^0(\mathbf{r},\mathbf{r}_1;\omega) \times V(\mathbf{r}_1,\mathbf{r}_2)\chi(\mathbf{r}_2,\mathbf{r}';\omega), \tag{2}$$

where $\chi^0(\mathbf{r},\mathbf{r}';\omega)$ is the response function for noninteracting electrons, which will be defined below, and $V(\mathbf{r}_1,\mathbf{r}_2)=1/|\mathbf{r}_1-\mathbf{r}_2|$ is the bare Coulomb potential.

Considering the periodicity on the plane of the ML we introduce a two-dimensional Fourier transform of the density response function,

$$\chi(\mathbf{r},\mathbf{r}',\omega)=\frac{1}{S}\sum_{\mathbf{q}}^{2\mathrm{DBZ}}\sum_{\mathbf{G},\mathbf{G}'}e^{-i(\mathbf{q}+\mathbf{G})\cdot\mathbf{x}}\times\chi_{\mathbf{G},\mathbf{G}'}(\mathbf{q},z,z';\omega)e^{i(\mathbf{q}+\mathbf{G}')\cdot\mathbf{x}'},\qquad(3)$$

where S represents the normalization area, the first sum runs over $\mathbf{q}$ vectors within the two-dimensional Brillouin zone (2DBZ), $\mathbf{G}$ and $\mathbf{G}'$ are reciprocal two-dimensional lattice vectors of the ML, and $\mathbf{x}$ and $\mathbf{x}'$ correspond to vectors lying on the plane parallel to the ML. Inserting Eq. (3) into Eq. (2) leads to the matrix equation

$$\chi_{\mathbf{G},\mathbf{G}'}(\mathbf{q},z,z';\omega)=\chi^0_{\mathbf{G},\mathbf{G}'}(\mathbf{q},z,z';\omega)+\sum_{\mathbf{G}_1}\sum_{\mathbf{G}_2}\int dz_1\int dz_2\chi^0_{\mathbf{G},\mathbf{G}_1}(\mathbf{q},z,z_1;\omega)\times V_{\mathbf{G}_1,\mathbf{G}_2}(\mathbf{q},z_1,z_2)\chi_{\mathbf{G}_2,\mathbf{G}'}(\mathbf{q},z_2,z';\omega),\qquad(4)$$

where $V_{\mathbf{G}_1,\mathbf{G}_2}(\mathbf{q},z_1,z_2)=2\pi\delta_{\mathbf{G}_1,\mathbf{G}_2}\,e^{-|\mathbf{q}+\mathbf{G}_1||z_1-z_2|}/|\mathbf{q}+\mathbf{G}_1|$ represents the two-dimensional Fourier transform of the Coulomb interaction potential. Fourier transforms of the response function of the noninteracting electron system have the well-known form[1]

$$\chi^0_{\mathbf{G},\mathbf{G}'}(\mathbf{q},z,z';\omega)=\frac{2}{S}\sum_{\mathbf{k}}^{2\mathrm{DBZ}}\sum_{n,n'}\frac{f_{\mathbf{k},n}-f_{\mathbf{k}+\mathbf{q},n'}}{E_{\mathbf{k},n}-E_{\mathbf{k}+\mathbf{q},n'}+(\omega+i\gamma)}\times\langle\phi_{\mathbf{k},n}|e^{-i(\mathbf{q}+\mathbf{G})\cdot\mathbf{x}}|\phi_{\mathbf{k}+\mathbf{q},n'}\rangle\times\langle\phi_{\mathbf{k}+\mathbf{q},n'}|e^{i(\mathbf{q}+\mathbf{G}')\cdot\mathbf{x}}|\phi_{\mathbf{k},n}\rangle,\qquad(5)$$

where the second sum runs over the band structure for each wave vector $\mathbf{k}$ in the 2DBZ, $f_{\mathbf{k},n}$, are the Fermi factors, $E_{\mathbf{k},n}$ represent the one-particle eigenvalues, and $\phi_{\mathbf{k},n}$ the corresponding eigenfunctions of the ground state.

We consider a perturbing positive charge located far from the ML, $z_0\gg d$ (d being the thickness of the ML). The differential cross section (loss function) for a process in which the electron is scattered with energy ω and momentum transfer $\mathbf{q}$ ($\mathbf{q}$ belonging to the 2DBZ) is proportional to $\mathrm{Im}\,g(\mathbf{q},\omega)$, where $g(\mathbf{q},\omega)$ is defined as the response function of a ML,[7–9]

$$g(\mathbf{q},\omega)=-\frac{2\pi}{|\mathbf{q}|}\int dz\int dz'\,\chi_{\mathbf{G}=0,\mathbf{G}'=0}(\mathbf{q},z,z';\omega)e^{|\mathbf{q}|(z+z')},\qquad(6)$$

which only depends on the electronic properties of the ML.

We use a local density approximation in order to calculate the total energy and one-particle eigenvalues and corresponding wave functions of free ML's. These quantities are evaluated with Troullier-Martins pseudopotentials[10] by using a supercell containing $L=40$ a.u. of vacuum in the direction perpendicular to the ML. In this approach, the Fourier transform of the electronic potential of electrons located at neighboring layers is given by $2\pi e^{-|\mathbf{q}|L}/|\mathbf{q}|$, which decays exponentially with $|\mathbf{q}|L$. Therefore, although the interlayer spacing used in the *ab initio* calculation is large ($L\gg d$), for very small momentum transfers ($|\mathbf{q}|<1/L$) electrons can feel the interaction with other layers and collective excitations show a three-dimensional character. As we are interested in analyzing the intrinsic two-dimensional characteristics of ML's, calculations will be restricted to momenta $|\mathbf{q}|>1/L$. The number of bands n required in the evaluation of $\chi^0_{\mathbf{G},\mathbf{G}'}$ in Eq. (5) depends on the value of the frequency ω, and we have checked that the results presented below are well converged when $\sim$ 80 bands are included. The sampling of the 2DBZ used for the evaluation of the response function in Eq. (5) is $\sim$7700. In the present work we avoid, however, direct use of Eq. (5), doing faster calculations of the spectral function matrix according to the approach described in Refs. 11 and 12 which is used for evaluation of imaginary and real parts of $\chi^0_{\mathbf{G},\mathbf{G}'}$ matrices.

III. CALCULATION RESULTS AND DISCUSSION

In this section we present the results for the electronic response for freestanding hexagonal ML's of lithium, beryllium, and boron as well as for graphitelike honeycomb ML's of boron.

A. Lithium monolayer

At equilibrium lithium ML forms the compact hexagonal structure, the energy difference with respect to the stabilized

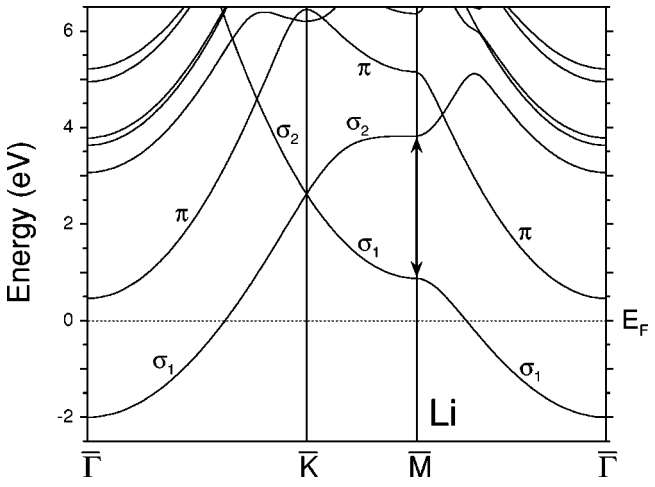

FIG. 1. Band structure of the compact hexagonal lithium ML. The Fermi energy is shown by the dotted line. Although the occupied band has essentially free-electron-like dispersion, the gap at $\bar{M}$, indicated by the arrow, is notably large as a result of the high nonlocal atomic pseudopotential. The various parameters are as follows: $m^*_{\sigma_1}=1.45$ and the Fermi momentum in the $\bar{\Gamma}\bar{K}$ direction is $k_{\mathrm{F},\sigma_1}=0.52$ a.u.$^{-1}$.

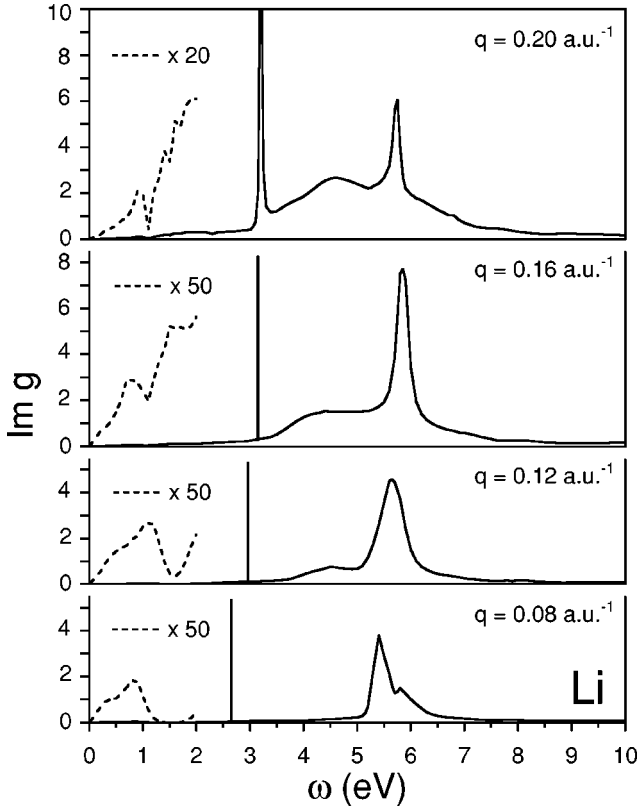

FIG. 2. Loss function $\mathrm{Im}\, g(\mathbf{q},\omega)$ of the hexagonal lithium ML for four different values of $|\mathbf{q}|$ in the $\overline{\Gamma K}$ direction. The main two peaks are associated to intraband and interband collective excitations, and the detailed spectrum (dashed lines) allows us to analyze the contribution associated with particle-hole excitations.

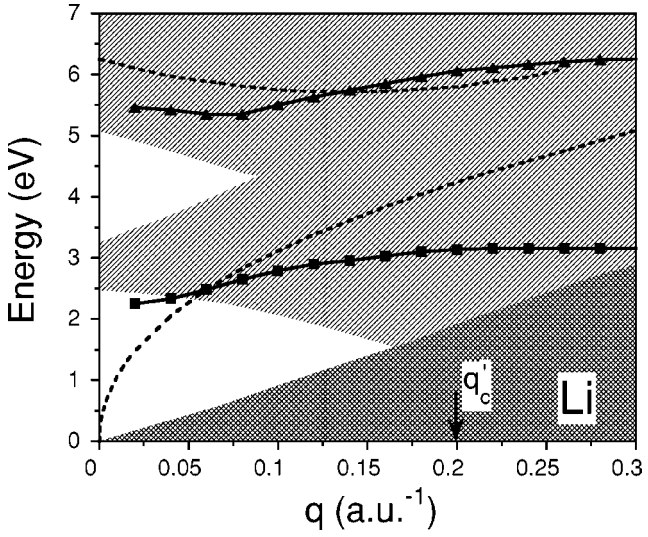

FIG. 3. Dispersion curves of the *ab initio* collective intraband (squares) and interband (triangles) excitations in the $\overline{\Gamma K}$ direction. For comparison, dashed lines show the plasmon dispersion curves evaluated within the free-electron-gas model by using the *ab initio* parameters. The hatched areas denote the regions where intraband (cross-hatched) and interband (line-hatched) particle-hole excitations are allowed. Although the intraband plasmon enters the interband excitation area at $|\mathbf{q}|\sim 0.05$ a.u.$^{-1}$, corresponding to $\sigma_1\rightarrow\pi$ interband particle-hole excitations, it does not decay until $|\mathbf{q}_c'|\sim 0.2$ a.u.$^{-1}$, where it begins to have finite linewidth because of the coupling to the interband $\sigma_1\rightarrow\sigma_2$ particle-hole excitations.

square structure being $\sim$ 0.2 eV/atom. The nearest-neighbor distance in the ML is 3.07 Å whereas for bulk it is 3.03 Å and the corresponding two-dimensional electronic density parameter is $r_s=3.02$ a.u.[13] In Fig. 1 we show the band structure of the lithium ML. As expected, the occupied lowest band is σ like and is characterized by an effective mass of $m^*_{\sigma_1}=1.45$. As a result of the high nonlocal pseudopotential, the energy gap at $\overline{M}$ ($\sim$3 eV) is comparable to the occupied bandwidth. The bottom of the next-highest band labeled by π is found at 0.34 eV above the Fermi energy (E_F), and this state has a π character.

In Fig. 2 we display the loss function of the lithium ML for selected wave vectors in the $\overline{\Gamma K}$ direction. As collective excitations will be mainly analyzed, small momentum transfers ($1/L=0.025$ a.u.$^{-1}<|\mathbf{q}|<k_F=0.52$ a.u.$^{-1}$) are considered. As $|\mathbf{q}|<1/L$ is much smaller than the characteristic Fermi momentum of the monolayers, we do not expect important quantum effects to happen in this range but just the classical $\sqrt{|\mathbf{q}|}$ dispersion of two-dimensional plasmons would be recovered. The main spectral weight corresponds to two plasmon peaks, but a more detailed spectrum also allows us to analyze the structure of particle-hole excitations. The first main peak at energy $\sim$3 eV corresponds to the intraband collective excitation, and the second one with energy of $\sim$5.5 eV is associated with the interband plasmon, which physically corresponds to the collective motion of electrons in the direction perpendicular to the ML. There are two main ranges in frequency where single-particle excitations contribute significantly (see Fig. 3). For small energies the contribution corresponds to intraband excitations. This region is denoted by the dark gray area. At higher energies one can see the contributions (shown in light gray) associated with interband excitations.

From the location of the different peaks in the dynamical response function we plot in Fig. 3 the dispersion curves of both collective excitations. In this figure, we also present for comparison the dispersion relations of both plasmons for a free-electron ML of finite thickness d within the jellium model when just the first two bands are included.[14] The value of $d\sim 10.5$ a.u. has been chosen so that the energy difference between the first two bands obtained within the infinite barrier approximation, $E_{12}=3\pi^2/2m_1^*d^2$, corresponds to the *ab initio* band structure calculation. Within this model, in the long-wavelength limit the intraband plasmon can be approximated by $\omega_{\mathrm{intra}}=\omega_{2\mathrm{D}}(1-0.1035|\mathbf{q}|d)$ (see Ref. 15), where the first term gives the plasmon dispersion for the strictly two-dimensional electron gas, $\omega_{2\mathrm{D}}=[2E_\mathrm{F}|\mathbf{q}|+(3E_\mathrm{F}/2m_1^*)|\mathbf{q}|^2+O(|\mathbf{q}|^3)]^{1/2}$ (see Ref. 2), and the second term represents the form factor correction corresponding to the finite width of the ML. As the electronic wave functions belonging to different bands have an alternative symmetry along the direction perpendicular to the ML, the intraband plasmon is not coupled to $\sigma_1\rightarrow\pi$ interband excitations. Therefore, contrary to bulk lithium,[16] within the RPA the intraband plasmon

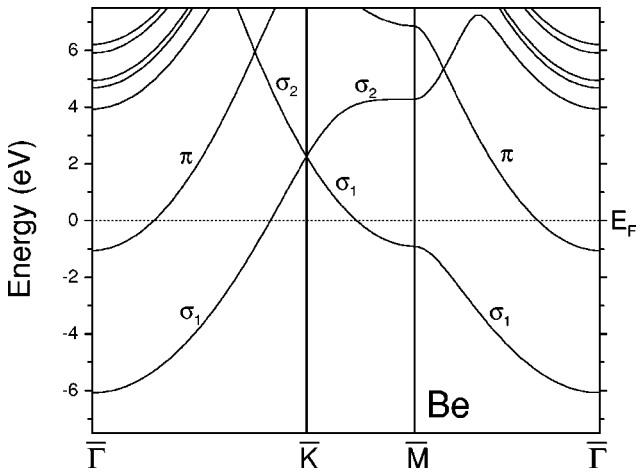

FIG. 4. Band structure of the hexagonal beryllium ML. The various parameters are as follows: $m^*_{\sigma_1}=1.48$, $m^*_{\pi}=1.04$ and the Fermi momenta along $\overline{\Gamma K}$ direction are $k_{\mathrm{F},\sigma_1}=0.81$ a.u.$^{-1}$ and $k_{\mathrm{F},\pi}=0.27$ a.u.$^{-1}$.

cannot decay because of the coupling with these excitations for small momenta. At the same time, as follows from Fig. 2, the intraband plasmon begins to have a finite linewidth for $q>q_c'=0.2$ a.u.$^{-1}$, significantly before the entering to the intraband particle-hole excitation region at momentum q_c. The origin of this decay is the coupling with the $\sigma_1\rightarrow\sigma_2$ interband excitations. On the other hand, the energy of the interband plasmon is proportional to E_{12} and the difference between the interband plasmon and E_{12} corresponds to the so-called depolarization shift. One can see that for small q the energies of the collective interband excitations are about 2 times ($\sim$2.2) as high as the interband single-particle $\sigma_1\rightarrow\pi$ excitations. In the long-wavelength limit the interband plasmon dispersion is negative, which is also reproduced within the free-electron-gas model and is a common feature of surface plasmons of alkali metals.[9] Contrary to the intraband collective excitation, the interband plasmon presents a finite lifetime even at $q=0$ due to its coupling to different interband particle-hole excitations.

B. Beryllium monolayer

As in the case of the lithium ML, a compact hexagonal structure also stabilizes the geometry of the berillium ML with an interatomic distance of 2.28 Å (2.29 Å for bulk) corresponding to an electronic density parameter of $r_s=1.6$. The band structure of the beryllium ML at equilibrium is shown in Fig. 4. In this case, because of the higher Be valence compared to Li, the second band π drops below the Fermi level, which significantly changes the electronic properties of the ML. Similarly to lithium, the first band has a σ character and the second one is π like, being antisymmetric in the perpendicular direction to the ML. The main modification of the effective mass compared with free-electron-gas dispersion corresponds to the first band ($m^*_{\sigma_1}=1.48$) while the π band is more free electron like ($m^*_{\pi}=1.04$) and the occupation of two bands implies the presence of two Fermi lines. The growing pseudopotential, as evidenced by the increasing gap at the $\overline{M}$ point ($\sim$5 eV), results in a full occupation of the first band around this point.

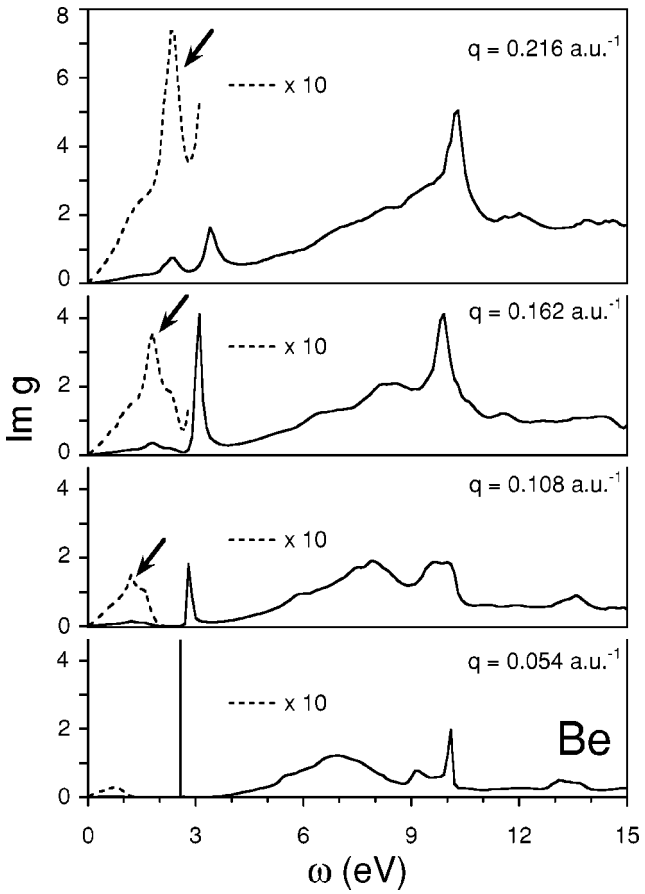

FIG. 5. Loss function of the beryllium ML for several momenta in the $\overline{\Gamma K}$ direction. Although main features are associated with 2D-like (intraband) plasmons at energy $\sim$3 eV and two different interband collective excitations with energies $\sim$8 eV and $\sim$10 eV, one can also see (as indicated by the arrows) a noticeable peak corresponding to the acoustic plasmon as a result of the presence of two types of electrons at the Fermi level.

The loss function calculated for the beryllium ML at selected momenta in the $\overline{\Gamma K}$ direction is displayed in Fig. 5. Corresponding particle-hole excitation regions and dispersion relations of the main collective excitations are presented in Fig. 6. Because of the presence of two partly occupied energy bands, the areas of intraband and interband particle-hole excitations are more complicated than in the case of the lithium ML. Thus, in Fig. 6 with dark and light gray colors we show particle-hole intraband and interband excitations, respectively, related to the σ_1 energy band, whereas two hatched areas denote corresponding regions for the π energy band. Besides the two plasmons that appear for the Li ML, here one can also see peaks associated with two other different interband collective excitations with energies $\sim$8 eV and $\sim$10 eV. While the two interband plasmons are highly coupled to interband single-particle excitations, the 2D-like intraband collective excitation only can decay at $|\mathbf{q}|>0.1$ a.u.$^{-1}$ by entering the $\sigma_1\rightarrow\sigma_2$ interband excitation area.

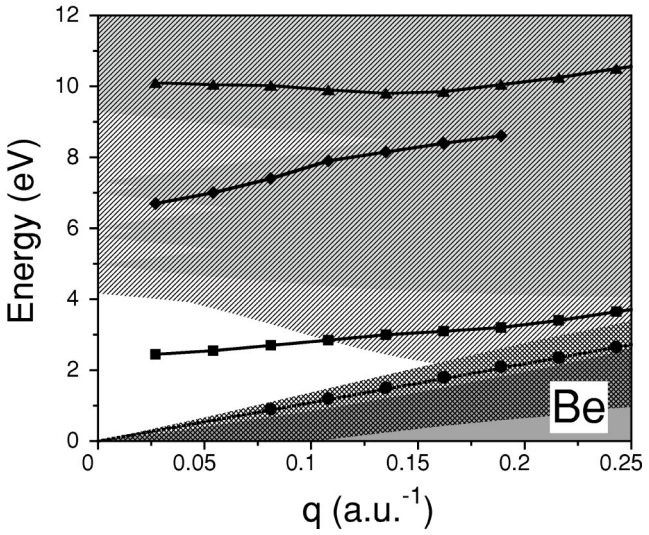

FIG. 6. Dispersion curves of the four collective excitations observed in the beryllium ML in the ΓK direction: the acoustic plasmon (solid circles) which is linear in $|\mathbf{q}|$ with a *sound* velocity of 0.4 a.u., a 2D-like intraband collective excitation (squares), and two different interband plasmons (diamonds and triangles). The hatched areas denote the regions where particle-hole intraband (cross-hatched) and interband (line-hatched) excitations are allowed for electrons in the σ_1 band. The lower shaded area represents the region for intraband excitations of electrons in the π band, while the upper one corresponds to the interband excitations of electrons in the same band.

But, again, as for the lithium ML, it happens for momentum $|\mathbf{q}|$ significantly smaller than q_c.

It is known that in the presence of electrons with different velocities at the Fermi energy, besides, the 2D-like collective excitation (at ~ 2 eV in the beryllium ML) also may exist an acoustic plasmon with a linear dispersion in $|\mathbf{q}|$.[17] In this case the light electrons can act to screen the Coulomb repulsion between the slower electrons originating the aditional intraband acoustic collective excitations. Normally, acoustic plasmons are strongly Landau damped by entering the intraband single-particle excitation region which highly depends on the characteristic band structure of the electronic system. However, peaks corresponding to the acoustic plasmon can be clearly distinguished in the berillium ML, as is indicated by arrows in Fig. 5. This is a signature that for this ML the conditions for the existence of this kind of collective electron motion may be satisfied. In contrast to 2D-like plasmons, which are well established experimentally,[4] the acoustic counterparts have not yet been unambiguously identified. Nevertheless, there are several speculations about their important role in changing the Coulomb pseudopotential associated with MgB_2 (Ref. 18) and intercalated layered metallochloronitrides (Ref. 19) superconductors.

C. Boron monolayers

Contrary to lithium and beryllium ML's, the geometry minimizing the energy of boron ML corresponds to the hexagonal honeycomb structure with an interatomic distance of 1.81 Å ($r_s = 1.27$ a.u.). The energy difference with respect to the closest competing structure (compact hexagonal with an interatomic distance of 1.69 a.u. and $r_s = 0.97$ a.u.) is $\sim$ 10 meV/atom. As is well known, the hexagonal honeycomb structure also minimizes the energy of graphite and with its three electrons per atom boron becomes the element of the row where the transition between both competing geometries takes place. Hexagonal honeycomb structure also stabilizes the geometry of boron layers in superconducting MgB_2 compound, with the smaller interatomic distance (1.78 Å) due to the increased binding charge density donated by magnesium atoms.

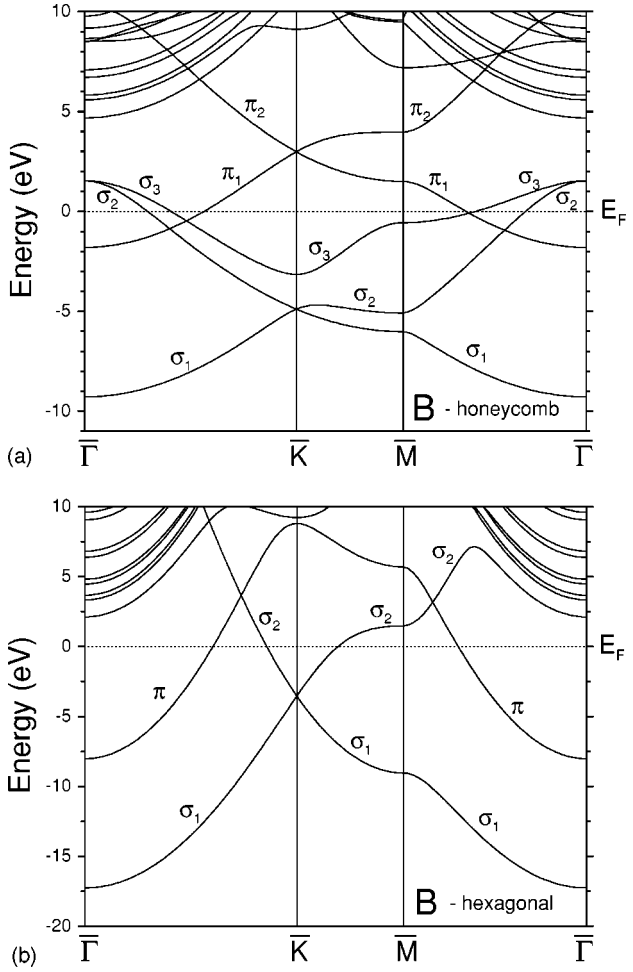

FIG. 7. Band structures of (a) honeycomb and (b) compact hexagonal boron ML's, respectively.

In order to analyze differences between both geometries, in Fig. 7 we present the band structures of each one at equilibrium. The symmetry of the lower two bands at the $\overline{\Gamma}$ point is similar to the ones of the ML's analyzed above. The loss function for several momenta in the $\overline{\Gamma K}$ direction of the 2DBZ corresponding to both boron ML's is shown in Fig. 8 and dispersion relations of the observed collective excitations are presented in Fig. 9. Because of the more complicated particle-hole excitation areas of these ML's compared with the cases of the lithium and beryllium ML's, they are

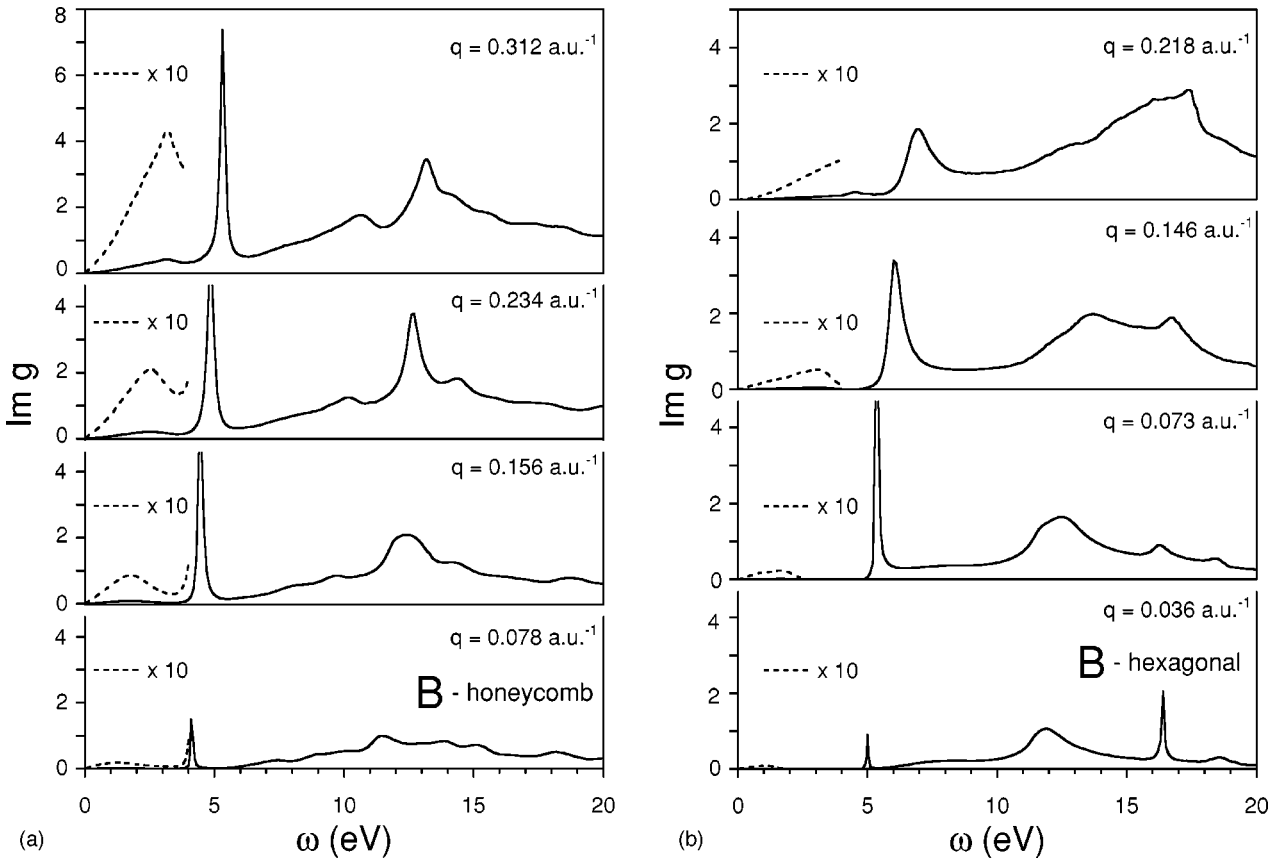

FIG. 8. Loss function of (a) honeycomb and (b) compact hexagonal boron ML's at selected momenta in the $\overline{\Gamma K}$ direction. Contrary to beryllium, there is no distinguishable peak associated with the acoustic plasmon.

not shown in Figs. 9(a) and 9(b). Although boron ML's also present two types of carriers at the Fermi level, as evidenced from Figs. 7(a) and 7(b), the corresponding acoustic plasmon is highly damped and indistinguished from single-particle excitations (see Fig. 8). Therefore, in boron ML's there is no evident sign of acoustic plasmons, which is also the case of MgB_2, and the main peaks are associated with one intraband and two interband plasmons that are damped beginning from relatively small values of $|\mathbf{q}|$ because of the decay to many intraband and interband particle-hole excitations. The decay

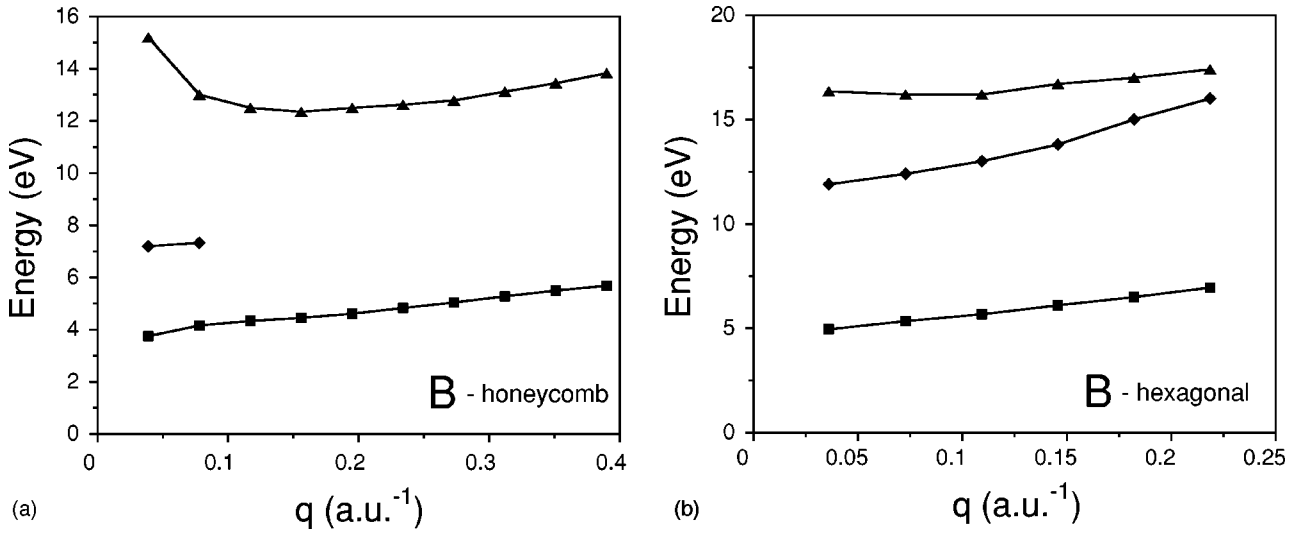

FIG. 9. Dispersion curves of the intraband collective excitation (squares) and two different interband plasmons (diamonds and triangles) associated with (a) honeycomb and (b) compact hexagonal boron ML's. The lower-energy interband plasmon of the honeycomb boron ML becomes highly damped and undistinguished for higher momenta.

rate of these collective excitations, which is proportional to the width of the peaks, increases with momentum, so that the first interband collective excitation in honeycomb boron ML is only well defined for small momenta. A similar spectrum with well-defined two peaks has also been predicted for superconducting MgB_2,[20,21] with two main collective excitations of energies $\sim 2-8$ eV and $\sim 18-22$ eV. The first collective excitation, which already exists in boron honeycomb ML as intraband plasmons, has also been observed in the hypothetical structure obtained from MgB_2 by removing the magnesium atoms,[20] thus manifestating the two-dimensional character associated with boron orbitals.

Considering that a perturbing external electron is located far from the ML, $z_0 \gg d$, one can define the induced density by[9]

$$\delta n(\mathbf{q},z;\omega)=\frac{2\pi}{|\mathbf{q}|}\int \mathrm{d}z' e^{|\mathbf{q}|z'}\chi_{\mathbf{G}=0,\mathbf{G}'=0}(\mathbf{q},z,z';\omega). \quad (7)$$

The breaking of the symmetry in the direction perpendicular to the ML has important advantages when analyzing the character of collective excitations. As is well known, wave functions associated with different bands have an increasing number of nodes in the z direction and, therefore, the contribution associated with each band, which highly depends on the geometry of the ML, can be easily deduced from the spatial symmetry of the electronic induced density corresponding to plasmons. When just two bands are partially occupied, the electronic density induced by the 2D-like intraband plasmon is symmetric with respect to the center of the ML:

$$\delta n_{\mathrm{intra}}(\mathbf{q},z;\omega)=\delta n_s(\mathbf{q},\omega)\,\eta_s^2(z)+\delta n_a(\mathbf{q},\omega)\,\eta_a^2(z), \quad (8)$$

where η_s (symmetric) and η_a (antisymmetric) are the wave functions in the z direction corresponding to the first and second bands, respectively, and δn_s and δn_a are the contribution weights of each band. In Fig. 10 we present the total induced density with $|\mathbf{q}|=0.156$ a.u.$^{-1}$ and $|\mathbf{q}|=0.073$ a.u.$^{-1}$ at the frequencies corresponding to the intraband plasmons in the honeycomb and hexagonal compact boron ML's, respectively. The asymmetry on the induced density is given by the contribution associated with intraband particle-hole excitations, which slightly moves the maximum to the side where the external perturbation is located. For the honeycomb structure the induced density presents a maximum at the center of the ML; however, it shows a minimum for the hexagonal compact structure. While the maximum at the center indicates that the main contribution is associated with the first band (σ plasmon) the presence of a minimum indicates the major role played by the the second band (π plasmon). Therefore, the change of the symmetry of the ML (while keeping the electronic density approximately the same) and the corresponding modification in the band structure completely modifies the spatial character of the intraband plasmon.

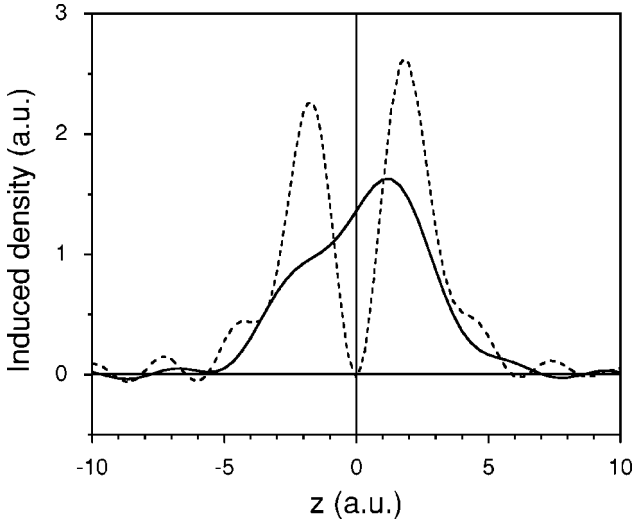

FIG. 10. Induced density profiles in the z direction for the honeycomb (solid line) and compact hexagonal (dashed line) boron ML's associated with the excitation of the corresponding intraband plasmons with $|\mathbf{q}|=0.156$ a.u.$^{-1}$ and $|\mathbf{q}|=0.073$ a.u.$^{-1}$, respectively, in the ΓK direction originated by an external perturbation.

IV. CONCLUSIONS

To summarize, we have performed *ab initio* calculations for the dynamical density response function of lithium, beryllium, and boron freestanding ML's by using density functional theory and the random-phase approximation. Although these density response functions share common properties associated with the reduced dimensionality—i.e., the presence of intraband and interband plasmons—they also show important differences resulting from their characteristic band structure. Contrary to the bulk, within the RPA long-wavelength intraband plasmons in lithium and beryllium ML's cannot decay via interband particle-hole excitations presenting, therefore, an infinite lifetime. At the same time, the presence of the interband $\sigma_1 \rightarrow \sigma_2$ particle-hole excitations leads to the appearance of the finite lifetime of these plasmons for significantly lower momentum compared with the nearly free-electron-like model. We have found peaks in the loss function of beryllium ML corresponding to the excitation of plasmons, associated with the presence of two types of electrons at the Fermi level; however, they become highly damped and undistinguished in boron ML's. On the other hand, we have shown that by changing the geometry of boron ML's the character of the observed collective excitations is completely modified. This analysis also allows us a better understanding of materials with a well-defined layered structure, as the MgB_2 superconductor.

ACKNOWLEDGMENTS

The authors acknowledge partial support by the University of the Basque Country, the Basque Hezkuntza, Unibertsitate eta Ikerketa Saila, the Spanish Ministerio de Educación y Cultura.

[1] See, e.g., D. Pines, *Elementary Excitations in Solids* (Addison-Wesley, New York, 1963).
[2] F. Stern, Phys. Rev. Lett. **18**, 546 (1967).
[3] T. Ando, A. B. Fowler, and F. Stern, Rev. Mod. Phys. **54**, 437 (1982).
[4] T. Nagao, T. Hildebrandt, M. Henzler, and S. Hasegawa, Phys. Rev. Lett. **86**, 5747 (2001); Surf. Sci. **493**, 680 (2001).
[5] R. Biagi, V. Corradini, G. Bertoni, C. Mariani, and U. del Pennino, Phys. Rev. B **64**, 195407 (2001).
[6] J. Nagamatsu, N. Nakagawa, T. Muranaka, Y. Zenitani, and J. Akimitsu, Nature (London) **410**, 63 (2001).
[7] B. N. J. Persson and E. Zaremba, Phys. Rev. B **31**, 1863 (1985).
[8] K. D. Tsuei, E. W. Plummer, A. Liebsch, E. Pehlke, K. Kempa, and P. Bakshi, Surf. Sci. **247**, 302 (1991).
[9] A. Liebsch, *Electronic Excitations at Metal Surfaces* (Plenum, New York, 1997).
[10] N. Troullier and J. L. Martins, Phys. Rev. B **43**, 1993 (1991).
[11] F. Aryasetiawan and O. Gunnarsson, Phys. Rev. B **49**, 16 214 (1994).
[12] V. P. Zhukov, F. Aryasetiawan, E. V. Chulkov, I. G. de Gurtubay, and P. M. Echenique, Phys. Rev. B **64**, 195122 (2001).
[13] Here we have defined the two-dimensional density parameter r_s by the relation $S/N=\pi(r_s)^2$ for N valence electrons in a ML of area S.
[14] J. K. Jain and S. Das Sarma, Phys. Rev. B **36**, 5949 (1987).
[15] E. H. Huang and S. Das Sarma, Phys. Rev. B **64**, 165409 (2001).
[16] K. Karlsson and F. Aryasetiawan, Phys. Rev. B **52**, 4823 (1995).
[17] D. Pines, Can. J. Phys. **34**, 1379 (1956).
[18] K. Voelker, V. I. Anisimov, and T. M. Rice, cond-mat/0103082 (unpublished).
[19] A. Bill, H. Morawitz, and V. Z. Kresin, Phys. Rev. B **66**, R100501 (2002).
[20] V. P. Zhukov, V. M. Silkin, E. V. Chulkov, and P. M. Echenique, Phys. Rev. B **64**, R180507 (2001).
[21] Wei Ku, W. E. Pickett, R. T. Scalettar, and A. G. Eguiluz, Phys. Rev. Lett. **88**, 057001 (2002).